Journal of Colloid and Interface Science 360 (2011) 15–25

Contents lists available at ScienceDirect

Journal of Colloid and Interface Science

www.elsevier.com/locate/jcis

Tuning the self-assembled monolayer formation on nanoparticle surfaces with different curvatures: Investigations on spherical silica particles and plane-crystal-shaped zirconia particles

Bernhard Feichtenschlager [a], Christoph J. Lomoschitz [a], Guido Kickelbick [b,*]

[a] Vienna University of Technology, Institute of Materials Chemistry, Getreidemarkt 9/165, 1060 Vienna, Austria
[b] Saarland University, Inorganic Solid State Chemistry, Am Markt Zeile 3, 66125 Saarbrücken, Germany

ARTICLE INFO

Article history:
Received 12 November 2010
Accepted 9 March 2011
Available online 21 March 2011

Keywords:
Nanoparticles
Surface-functionalization
Self-assembled monolayers
Silica
Zirconia
Mixed monolayers

ABSTRACT

The ordering of dodecyl-chain self-assembled monolayers (SAM) on different nanoscopic surfaces was investigated by FT-IR studies. As model systems plane-crystal-shaped ZrO_2 nanoparticles and spherical SiO_2 nanoparticles were examined. The type of capping agent was chosen dependent on the substrate, therefore dodecylphosphonic acid and octadecylphosphonic acid were used for ZrO_2 and dodecyltrimethoxysilane for SiO_2 samples. The plane ZrO_2 nanocrystals yielded more ordered alkyl-chain structures whereas spherical SiO_2 nanoparticles showed significantly lower alkyl-chain ordering. Submicron-sized silica spheres revealed a significantly higher alkyl chain ordering, comparable to an analogously prepared SAM on a non-curved plane oxidized Si-wafer. In the case of ZrO_2 nanocrystals an intense alkyl-chain alignment could be disturbed by decreasing the grafting density from the maximum of 2.1 molecules/nm^2 through the variation of coupling agent concentration to lower values. Furthermore, the co-adsorption of a different coupling agent, such as phenylphosphonic acid for ZrO_2 and phenyltrimethoxysilane for SiO_2, resulted in a significantly lower alkyl-chain ordering for ZrO_2 plane crystals and for large SiO_2 spherical particles at high grafting density. An increasing amount of order-disturbing molecules leads to a gradual decrease in alkyl-chain alignment on the surface of the inorganic nanoparticles. In the case of the ZrO_2 nanoparticle system it is shown via dynamic light scattering (DLS) that the mixed monolayer formation on the particle surface impacts the dispersion quality in organic solvents such as *n*-hexane.

1. Introduction

Nanoparticle surface-functionalization is the major tool to increase the compatibility between these nano building blocks and their environment. Coupling agents are commonly applied for this approach [1]. These compounds consist of anchor groups that allow a stable attachment to the nanoparticle surface, a spacer, and optionally a functional group that permits further chemical interactions with the environment, e.g. a copolymerization in the formation of nanocomposites [2]. In many cases the spacer is a long alkyl chain that increases the compatibility of the often hydrophilic surface with hydrophobic media such as solvents, monomers, or polymers. Since many years it is known that such long alkyl chains can form self-assembled monolayers on flat substrates [3,4]. It was only recently that the effect of the nanocurved surface in case of nanoparticles became a topic of interest [5–8]. The question in this scope is whether there is a critical surface curvature, which leads to self-assembled monolayer formation [9], and how the thermodynamic driving force for such surface-aggregates can be reduced. One of the reasons why this becomes interesting is the formation of bilayers between different particles [10–12] leading to a formation of nanoparticle assemblies and thermodynamically stable agglomerates [8,13,14], which are undesirable in terms of the synthesis of homogeneous nanomaterials.

In this report we investigated the generation of self-assembled monolayers (SAMs) dependent on the structure and curvature of the nanoparticle surface. For this reason two different systems were evaluated, namely (i) spherical amorphous silica nanoparticles and (ii) crystalline zirconia nanoparticles. A recently published work on the SAM formation on the surface of silica particles showed a large effect of the curvature [9]. The aim of our study is the extension of the previous work to transition metal oxide nanoparticles with a focus on nonspherical crystalline systems, which often show planar crystal facets that mimic flat substrates on the macroscopic scale. We selected zirconia nanoparticles because of their importance as polymer fillers and the complementarity in surface chemistry compared to silica [15]. Long alkyl chain alkoxysilanes were used for the silica surface-functionalization while molecules with phosphonate

* Corresponding author.
E-mail address: kickelbick@mx.uni-saarland.de (G. Kickelbick).

0021-9797/$ - see front matter © 2011 Elsevier Inc. All rights reserved.
doi:10.1016/j.jcis.2011.03.035

anchor groups were applied for zirconia particles. Dodecyl alkyl chain containing coupling agents were selected because SAMs from these molecules are non-crystalline at room temperature [16,17] and therefore they less likely form very strong interparticle bilayers. This argument was proofed applying also a C18-phosphonic acid, which results in the formation of crystalline SAMs at plane surfaces below 50 °C [17] as disordering/ordering effects should appear more significantly in this system.

We also investigated methods to overcome strong alkyl-chain ordering phenomena in case of the model systems (i and ii) by mixed monolayer formation. The latter has been investigated until yet mostly for mixed alkyl thiols on gold nanoparticles [7] or to control the spacing between deposited particles [18]. The approach of generating mixed substituted surfaces was also investigated in the presented work to study its effect on the formation of dispersions in organic media, for example to improve the deagglomeration behavior of nanoparticles in dispersions. Prado et al. have studied the coadsorption approach on macroscopic flat surfaces for organophosphorus mixed monolayer [19] but this concept has not been applied to transition metal oxide colloids before.

2. Materials and methods

2.1. Materials

Dodecyltrimethoxysilane and phenyltrimethoxysilane were purchased from ABCR. All other solvents (HPLC grade) and chemicals were purchased from Sigma Aldrich and used as received. Methanol was purified using a PureSolv (Innovative Technology Inc.) solvent purification system. Phenylphosphonic acid was recrystallized from acetonitrile.

2.2. Instrumental analysis

Nitrogen sorption measurements were performed on a Micromeritics ASAP 2020 instrument at 77 K. The samples were degassed under vacuum at 60 °C for at least 8 h prior to measurement. The surface area was calculated according to *Brunauer*, *Emmett* and *Teller* (BET) [20]. Thermogravimetric analyses (TGA) were performed on a Netzsch Iris TG 209 C in a platinum crucible heating from room temperature to 900 °C with a heating rate of 10 °C/min under synthetic air. The grafting densities σ (molecules/nm^2) were calculated using the formula, as used in literature for similar systems [21].

$$\sigma = \frac{\Delta_m}{M_R} \cdot \frac{1}{S_{BET}} \cdot N_A \cdot 10^{-18} \quad (1)$$

where Δ_m is the mass loss from TGA between 200 °C and 800 °C (g/g) which is feasible because the onset of the thermal desorption for all used coupling agents was higher than 220 °C, M_R is the molecular mass of the organic moiety (g/mol), S_{BET} is the specific surface area from nitrogen sorption measurements of the bare metal oxide sample (m^2/g) and N_A is the *Avogadro*'s constant.

Fourier transform infrared spectroscopy (FT-IR) measurements were performed on a Bruker Tensor 27 Spectrometer under ambient air (64 scans at a resolution of 1 cm^{-1}) in transmission mode using KBr (Aldrich) disks as a sample matrix. For the investigation of monolayers on plane substrates the IRRAS-method (reflection–absorption-spectroscopy) has been applied using a Bruker Vertex 80 IR spectrometer.

Liquid state NMR spectra were recorded on a Bruker Avance 250 spectrometer (^{1}H at 250.13 MHz, ^{31}P at 101.26 MHz, ^{13}C at 62.80 MHz). Solid state NMR spectra were recorded on a Bruker Avance DPX 300 instrument equipped with a 4 mm broad band MAS probe head operating at 75.40 MHz for ^{13}C, at 121.39 MHz for ^{31}P and at 59.63 MHz for ^{29}Si. The ^{29}Si and ^{13}C spectra were recorded with ramped CP/MAS (cross polarization and magic angle spinning) and ^{31}P with HPDEC (high power decoupling) at a rotor frequency of 8 kHz. Elemental analysis was carried out at the Microanalytical Laboratory at the University of Vienna.

Powder XRD-measurements were carried out on a Philips X'Pert Pro instrument at Cu Kα – radiation with a *Bragg–Brentano*-arrangement and an angle speed of 6°/min where the sample was carried on Si single crystal wafers under ambient conditions.

Transmission electron microscopy (TEM) images were recorded on a JEOL JEM-100CX and on a FEI TECHNAI G20 transmission electron microscope. The samples were attached to Formvar copper grids by dispersing them in ethanol using an ultrasound cleaning bath, adding one drop on the copper grid and evaporating the solvent.

Dynamic light scattering (DLS) measurements were carried out by non-invasive backscattering on an ALV/CGS-3 compact goniometer system with an ALV/LSE-5003 correlator and multiple tau correlator at a wavelength of 632.8 nm (He—Ne Laser) and at a 90° goniometer angle. The dispersing media were purified before use with a syringe-filter (200 nm mesh). The determination of the particle radius was carried out by the analysis of the correlation-function via the g2(t) method followed by a linearized mass-weighting (m.w.) of the distribution function.

Ellipsometry measurements were carried out on a SENTECH SE500adv apparatus.

A Hettich EBA 20 S centrifuge (86 mm rotor radius) was used for the nanoparticle separation.

2.3. Synthesis of dodecylphosphonic acid

The coupling agent dodecylphosphonic acid was synthesized via an *Arbuzov*-reaction and hydrolysis of the obtained phosphonate was carried out applying literature-known procedures [22,23].

15.6 mL (64 mmol) 1-Bromododecane and 12.4 mL (74 mmol) triethylphosphite were stirred for 3.5 h under reflux. The excess of triethylphosphite was removed at 100 °C/12 mbar and the remaining intermediate product was afterwards refluxed with 70 mL HCl conc. for 22 h. The crude product was obtained as a white solid after concentrating the reaction mixture to 20 mL. The product was washed several times with acetonitrile and dried in an oil-pump-vacuum. It was further recrystallized from hexane and dried in an oil-pump-vacuum. Yield: 9.5 g (38 mmol, 59% of theory) colorless crystals.

Characterization:

^{1}H NMR($CDCl_3$): δ(ppm) = 0.84 (t, 3H, CH_3); 1.26 (m, 18H, CH_2); 1.55–1.82 (m, 4H, CH_2—CH_2—P); 8.56 (s, 2H, P—OH). ^{13}C NMR(DMSO-d6): δ(ppm) = 31.83, 30.52, 29.68–29.62 (6C), 26.63, 22.99 and 22.58 (CH_2); 14.22 (CH_3).
^{31}P NMR($CDCl_3$): δ(ppm) = 39.5.
IR (ATR): ν = 2954 cm^{-1} (CH_3); 2917 cm^{-1} (ν_{as} C—H, CH_2); 2871 cm^{-1} (CH_3); 2849 cm^{-1} (ν_s C—H, CH_2); 1469 cm^{-1} (C—H); 1212 cm^{-1} (P=O); 1003 cm^{-1} (P—O); 942 cm^{-1} (P—OH).

2.4. Nanoparticle synthesis

2.4.1. Silica nanoparticles

Silica nanoparticle sols have been prepared by the *Stöber*-process [24]. The nanoparticle preparations were carried out in 100 mL solvent by first adding water and NH_4OH to the solvent followed by the dropwise addition of tetraethyl orthosilicate (TEOS). The reaction mixtures were stirred at room temperature with a magnetic stirrer (600 rpm) for 2 days. Then the NH_3 was removed under oil-pump-vacuum and the amount of evaporated solvent

Table 1
Parameters in the *Stöber*-process to prepare silica particles.

H_2O (mL)	TEOS (mL)	NH_4OH conc. (mL)	Solvent	Particle diameter (DLS) m.w. (nm)
2.00	10.5	0.05	Methanol	9 ± 2
2.00	4.0	3.3	Ethanol	46 ± 10
2.00	6.0	12.0	Ethanol	390 ± 80
0.00	6.0	12.0	Ethanol	680 ± 55

was re-added to the mixture. This dispersion was directly used in the following *in situ* surface-modification step. Change of synthetic parameters, such as solvent type, amount of water, TEOS, and concentrated aqueous ammonia solution (Table 1), resulted in various silica particle diameters.

2.4.2. Zirconia nanoparticles

Zirconia nanoparticles were synthesized following a literature-known procedure [25] via thermal decomposition of 13 mL 4 M solution of $ZrOCl_2$ in water in an autoclave with a 20 mL-Teflon-inlay at 200 °C. The reaction was carried out for 3 days and the particles were isolated by precipitation with acetone and centrifugation at 6000 rpm. Afterwards they were washed with a mixture of water and ethanol (1:5) three times and dried over P_2O_5 at 5 mbar to yield 3.5 g of a white powder.

Characterization:

Powder-XRD: 100% crystalline ZrO_2, Baddeleyite phase (monoclinic), crystallite size (refinement using five metric parameters, software "TOPAS") 4–10 nm.
DLS: hydrodynamic diameters in water: 22 ± 7 nm mass weighted, 18 ± 4 nm number weighted.
TEM: crystals with aspect ratio of ~2, spherical equivalent diameter of 10 ± 2 nm (number weighted).
S_{BET}: 140 m^2/g.

2.5. Surface modification

2.5.1. Silica nanoparticles

Silica nanoparticles were modified using an *in situ* approach where 0.1 mL NH_4OH conc. was added to the freshly prepared silica sol under stirring, followed by the addition of dodecyltrimethoxysilane resulting in a 7.5 mM solution and further stirring for 2 days. Afterwards the particles were isolated by concentrating the dispersion via solvent removal and centrifugation at 6000 rpm. The particles were washed three times with maximum five milliliters of ethanol (centrifugation at 6000 rpm) and dried over P_2O_5 at 5 mbar for 24 h.

Characterization: dodecyltrimethoxysilane@SiO_2 (9 nm diameter):

IR: ν = 2929 cm^{-1} (ν_{as} C—H, CH_2); 2855 cm^{-1} (ν_s C—H, CH_3); 1461 cm^{-1} (C—H); 1091 cm^{-1} (Si—O).
^{13}C Solid State NMR: δ(ppm) = 28.0–20.4 (CH_2); 17.0 (CH_3); 11.2(Si—CH_2).
^{29}Si Solid State NMR: δ(ppm) = −61.9 (T); −69.6 (T); −97.3(Q); −105.5 (Q); −114.3 (Q).
TGA: Δm (200–800 °C) = 18.5%, Onset: 227 °C.
Elemental analysis: 8.9%C, 3.4%H (the higher H/C ratio origins from residual ethoxy-groups in the bulk material).

2.5.2. Zirconia nanoparticles

Zirconia nanoparticles were modified using a *post*-modification approach as described in literature for titanium dioxide nanoparticles [26]. First 5 mL of 10 g/L aqueous nanoparticle dispersion was prepared by dispersing the zirconia nanoparticle powder for 30 min in an ultrasonic bath. Afterwards HCl conc. was added dropwise to the dispersion to adjust the pH to 2. The phosphonic acid, e.g. 18.7 mg dodecylphosphonic acid for a 7.5 mM total coupling agent concentration, was dissolved in 5 mL methanol, added to the particle dispersion and the mixture was stirred for 2 days. Afterwards the particles were isolated via centrifugation at 6000 rpm, washed three times with ethanol and dried over P_2O_5 at 5 mbar for 24 h.

Characterization: dodecylphosphonic acid@ZrO_2:

IR (ATR): 2921 cm^{-1} (ν_{as} C—H, CH_2); 2851 cm^{-1} (ν_s C—H, CH_3); 1464 cm^{-1} (C—H); 1034 cm^{-1} (P—O broad).
^{13}C Solid State NMR: δ(ppm) = 30.0–19.5 (CH_2); 15.0 (CH_3).
^{31}P Solid State NMR: δ(ppm) = 27.0 (bs).
TGA: Δm (200–800 °C) = 14.5%, Onset: 268 °C.
Elemental analysis: 12.95%C, 2.45%H, 2.3%P.

2.6. Plane silica substrate

A plane silica substrate, a Si-wafer from Wacker Siltronic AG, fz, orientation 100, phosphorus doped, resistivity $\geqslant$4500 Ω cm has been oxidized using a piranha-solution. The thickness of the SiO_2 film was determined by ellipsometry to be 137 ± 3 pm. The functionalization reaction was carried out under the same conditions as described for silica nanoparticles.

3. Results and discussion

3.1. Nanoparticle systems

In order to investigate the self-assembly phenomena on nanoscale surfaces, two different model systems were synthesized: spherical amorphous silica nanoparticles on the one hand, and plane shaped crystalline zirconia nanoparticles on the other hand. The silica particles were prepared in different diameters to correlate the self-assembly behavior with their nanoscopic curvature.

While the synthesized zirconia nanoparticles consisted of phase pure monoclinic ZrO_2 (Baddeleyite) as investigated by *Rietveld*-refinement (diffractogram and comparison diagram see Supplemental information, Fig. SI 2) all silica particles were X-ray amorphous in nature.

The physical habit and morphology of the particles was investigated by TEM and DLS. The TEM image (Fig. 1) of ZrO_2-nanoparticles reveals a uniform size and shape of the particle fraction, the selected area electron diffraction pattern shows the typical sharp diffraction lines for highly crystalline materials. The particle size and crystal-shape observed in TEM in combination with the crystallite size of 4–10 nm calculated from the diffraction peak width caused by the sample indicates that the ZrO_2-nanoparticles were single nanocrystals (aspect ratio ~2). TEM images of the silica particles reveal a spherical morphology and uniform size (see Fig. 2 left).

DLS-measurements have been performed for a better representation of the whole particle collective in form of a size distribution diagram. Calculations from DLS data with regard to the size distribution are based on the model of a spherical morphology of the nanoparticles which is the case for SiO_2 (Fig. 1) but not for ZrO_2 (Fig. 2). Therefore the data for zirconia represents spherical equivalent radii (Fig. 3a). Fig. 3b shows the uniform size distributions of the synthesized SiO_2-model-(nano)particles.

Based on these well defined zirconia and silica (nano)particles detailed investigations on the attachment of coupling agents were carried out.

3.2. Anchoring of coupling agents to the nanoparticle surface

Trialkoxysilanes are well known for their affinity to silica surfaces and were used in a plethora of self-assembly studies particularly on flat substrates [3,4]. The silane coupling agents also have an affinity to metal oxide surfaces. However, the stability of Si—O—M bonds is in some cases low, for example against hydrolysis. Phosphonates show a much higher stability to metal oxide surfaces and are therefore quite often used as anchor groups [15,27]. Table 2 lists the coupling agents which have been used in our studies. Silane coupling agents of the type R-SiX_3 covalently bind with a maximum of 3 Si—O—Si bonds to the surface and a cross condensation of coupling agent molecules is possible [28]. Depending on the degree of this homocondensation, the amount of surface bound groups can be rather low even in a dense monolayer. Phosphonic acids covalently bind to many metal oxide surfaces. Detailed studies can be found in literature for titania surfaces [29]. The binding mechanisms usually involve one to three M—O—P bonds and are expected to be similar for zirconia. In both cases the kinetics for the anchoring reactions for phosphonates@zirconia [30] and alkoxysilanes@silica [31] is very fast. Therefore a maximum possible grafting density can be assumed for each performed modification reaction. Our studies focus on C12 chains because we want to concentrate on non-crystalline surface-SAMs. C18 chain capping molecules have just been used for demonstration issue to show the transferability of the here observed effects to other systems.

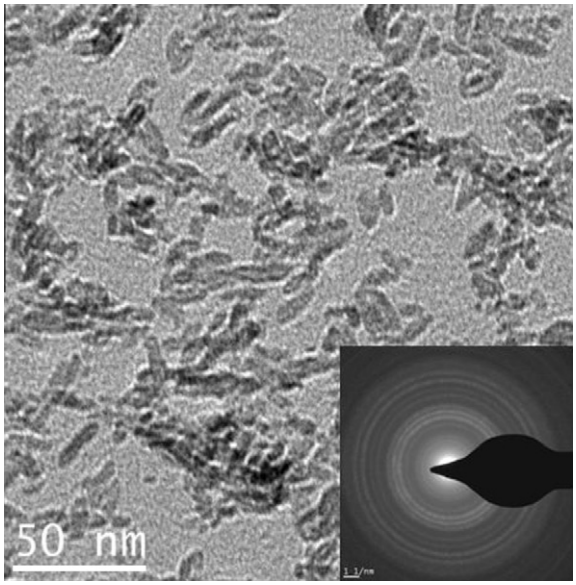

Fig. 1. Zirconia with specific nanoscopic curvature: TEM image of ZrO_2 nanoparticles and SAED-pattern.

Beside covalently bound monolayers of the coupling agents additional physisorbed molecules can be excluded due to the intense washing steps after modifying the surface and because there was no spectroscopic evidence for physisorbed molecules by IR and solid state NMR.

The degree of ordering of the molecules on the surface of the nanoparticles has been investigated applying IR spectroscopy. Following a method used for the detection of self-assembled monolayers (SAM) a redshift of the long alkyl chain methylene group C—H-vibration due to a decrease of gauche defects indicates a higher ordering in the SAM and thus a more dense chain packing [32,33]. The asymmetric C—H-stretching mode of the chain methylene unit is the most significant resonance where the peak value is used to monitor the degree of chain ordering [30].

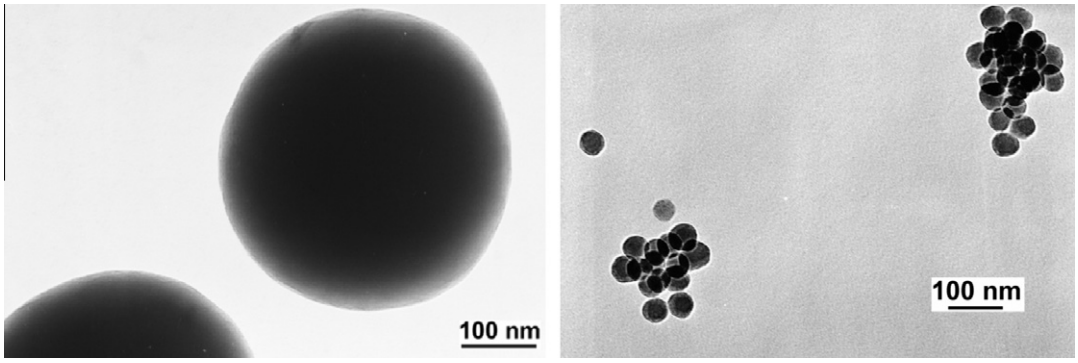

Fig. 2. TEM images of SiO_2 nanoparticles with different curvature: left – 390 nm diameter particle fraction, 46 nm diameter particle fraction.

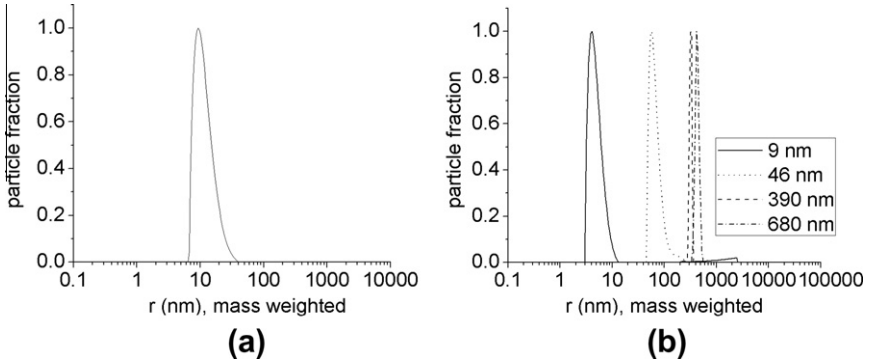

Fig. 3. Particle size distribution of ZrO_2 nanocrystals in water (a) and particle size distributions of SiO_2 in various sizes (diameter from peak) in ethanol (b).

Table 2
Studied surface modifying agents.

Coupling agent formula	Coupling agent name	Abbreviation
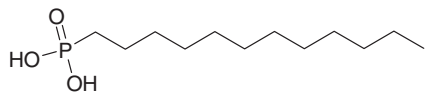	Dodecyl phosphonic acid	DPPA
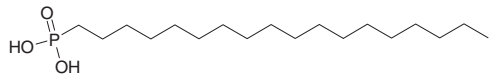	Octadecyl phosphonic acid	ODPPA
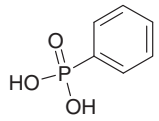	Phenyl phosphonic acid	PhPPA
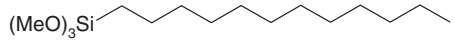	Dodecyl trimethoxysilane	DTMS
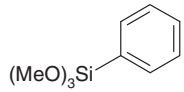	Phenyl trimethoxysilane	PhTMS

3.3. Zirconia nanocrystals: grafting density and alkyl-chain ordering

The grafting density has been varied using different concentrations of the coupling agent DPPA in the reaction mixture to investigate how grafting density effects the ordering of the alkyl-chains attached to the nanoparticle surface. Fig. 4 shows the results for the grafting densities at different coupling agent concentrations in the reaction solution calculated from mass loss from TGA and specific surface area from nitrogen sorption measurements. The maximum grafting density was determined to be 2.1 molecules/nm^2 for DPPA@ZrO_2 and 3.4 for ODPPA@ZrO_2 because C18-SAMs are usually more ordered and thus more closely packed. Nevertheless, the maximum grafting density for phosphonates at a plane metal oxide surface has been reported to be 4.2–4.8 molecules/nm^2 for the dense C18-monolayer [30,34]. The difference in these values can be partially explained by the fact that Fadeev et al. assume a surface demand of N_2 molecules of 0.135 nm^2 for the calculation of the specific surface area from their nitrogen sorption experiments. Whereas we assume a demand of 0.162 nm^2 which results in a higher specific surface area of the nanopowder and therefore our values for the grafting densities are lower by a factor of 0.83. In addition also the variations in the morphology of a metal oxide nanoparticle surface compared to a macroscopically plane surface can be responsible for the lower, grafting densities. Nanoparticle surfaces exhibit a high curvature with many defects and disordering phenomena. Furthermore very often particles show an amorphous outer-shell-formation at their surface which has to be taken into account if the surface is compared with an ideal crystal surface [35]. Also the number of surface OH-groups responsible for chemical bonding between organophosphorus anchor groups and the various oxidic nanoparticle surfaces usually differs from the coordination site number on a perfect plane surface [36], which has negative impact on the grafting density. Also a systematic error for all series has to be taken into account, namely how good the BET surface value represents the real surface area of the nanoparticles, which is accessible for the functionalization. The BET surface area can underestimate the total accessible area because the surface is partially nonaccessible for nitrogen in the dried powder but is accessible for the capping agent in the reaction dispersion. Hence the grafting density values would be higher in reality. This error is considered to be low in the range of the measurement accuracy because the nitrogen adsorption/desorption isotherm together with the developed pore size distribution show only mesopores (detailed explanation and figures see Supplemental data).

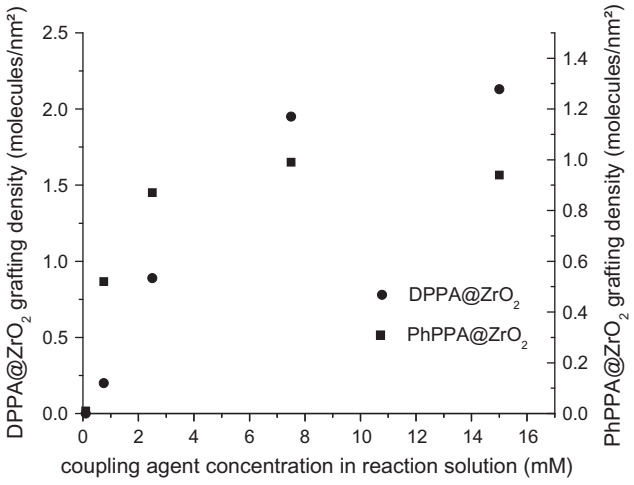

Fig. 4. Effect of the coupling agent concentration (DPPA or PhPPA) in the reaction mixture on the zirconia nanoparticle surface coverage with DPPA or PhPPA.

PhPPA shows a maximum grafting density of approximately 1 molecule/nm^2, which is much lower compared to the long alkyl chain DPPA molecules due to the lack of SAM formation in this case [37].

The correlation of coupling agent concentration and the resulting grafting density is shown in Fig. 4 for DPPA@ZrO_2 and for PhPPA@ZrO_2. The diagram reveals that with increasing coupling agent concentration the grafting density increases nearly linearly until the surface seems to reach saturation (plateau for grafting density for PhPPA ~ 1 molecule/nm^2 and for DPPA ~ 2 molecules/nm^2) at a threshold of ~7.5 mM for both coupling agent molecules. In literature similar characteristics have been observed for bulky phosphorus coupling-agents attached to zirconia nanoparticle surfaces where the adsorpion-isotherm shows *Langmuir*-characteristics [38]. Fig. 4 can therefore also be interpreted as an adsorption isotherm where every datapoint represents an equilibrium grafting density.

The ordering degree of the dodecyl chains on the particle surface has been investigated via IR spectroscopy. The values for the asymmetric stretch vibration ν_{as} of the methylene-chain C—H-bond in Fig. 5 visualize the observed shift to lower C—H wavenumbers for higher grafting densities. The lowest wavenumber in the

investigated sample was 2922 cm^{-1} at maximum grafting density (highest ordering). This wavenumber is considerably higher than those of ideal SAMs reported in literature, e.g. C_{17}-thiol@gold shows a C—H-wavenumber of 2917 cm^{-1} [39] and C18-organosilanes@zirconia 2916 cm^{-1} [21]. Explanations for the differences in packing and the lower ordering in the case of our systems are the already mentioned differences between flat substrates and nanoparticles surfaces and the more dense packing of longer alkyl chains (C17 and C18 compared to C12) which is a commonly known phenomenon [37]. Gao et al. have investigated the microcrystallinity of SAMs of alkylphosphonates with different chain length on ZrO_2. They have shown that below 50 °C, where also our preparation steps were carried out, only alkyl chains longer than 16 C-atoms per chain form real crystalline surface SAM structures [17]. C12-chains as applied in our work form packings, but in a more disordered way. All chain methylene-units can be in the all *trans* configuration, but more disordered as in a crystal [16].

The results on the nanoscopic surface reveal that higher grafting density causes a higher ordering of the alkyl-chains attached to the surface. Similar observations were described in literature for long alkyl chain trialkoxysilanes or phosphonic acids at micrometer powder surfaces of silica, titania, zirconia, hafnia [21,30,32,37] where larger flat surface areas compared to nanoparticles can be formed. However, no conclusion about the consistency of the monolayers with different grafting densities can be drawn from the absolute values of C—H-shifts. On not fully covered surfaces the coupling agent can be randomly attached, which is more likely for phosphonates than for trialkoxysilanes [30], because the trialkoxysilanes form preordered structures via cross-condensation of the anchor groups already in solution before they adsorb to the particle surface. Therfore they can form a number of small islands or a mixture of both [30].

It can be concluded from these results that a 7.5 mM concentration of DPPA leads to a dense SAM for this particle type. Below this concentration lower ordered alkyl-chain structures are formed at the surface as IR measurements indicate (Fig. 4).

Variation of the coupling agent concentration is a method to tune the SAM-formation on the surface (Fig. 5 shows the different alkyl-chain ordering states for different grafting densities). This is important because SAM-functionalized particles can interact with each other through bilayer formation. Such bilayers are thermodynamically very stable and therefore it is difficult to separate agglomerated particles showing this effect.

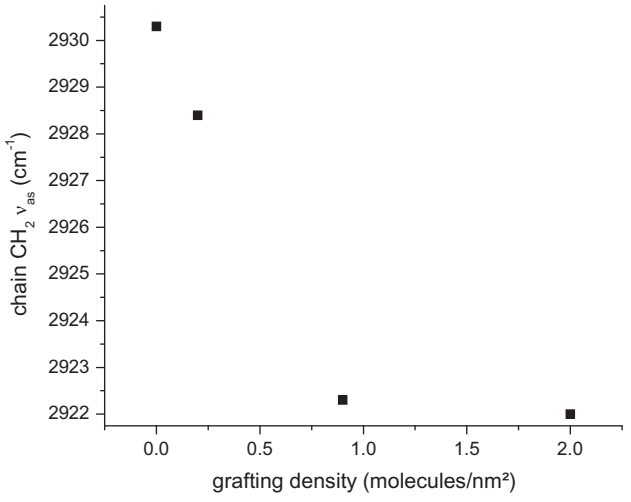

Fig. 5. Different grafting densities of DPPA@ZrO_2, ν_{as} CH-wavenumber represents the ordering degree of the alkyl-chains (chain packing).

3.4. Zirconia nanocrystals: alkyl chain disordering by co-modification

A method to tune the alkyl-chain ordering while having a certain constant coverage of molecules on the nanoparticle surface is to mix two different coupling agents consisting of the same anchor group but showing organic substituents of different chemical nature, such as a dodecyl chain and a phenyl group. The coupling agent presenting a smaller organic group can disturb the long-alkyl-chain SAM formation process. This approach was investigated by mixing DPPA and PhPPA in certain ratios to give an altogether 7.5 mM solution of phosphonic acid coupling agents which represents the threshold-concentration for a dense monolayer formation. This concentration has been chosen to exclude a significant preferential adsorption and binding of one of the different coupling agents which would lead to higher surface concentrations of one type of molecule. The reason for this approach is that phenylphosphonic acids are known to be more reactive than alkylphosphonic acids towards binding to metal oxide surfaces [29]. Also it is known from literature that in a coupling agent mixture which forms a mixed monolayer smaller molecules are faster adsorbed to the surface as Offord and Griffin have shown for mixed layers of homologous *n*-alkyltrimethoxysilanes on a plane silica surface [40]. The mixture was used for surface modification to prepare 10%, 30%, 50%, 70%, 90%, 100% DPPA@ZrO_2 where the difference to 100% is PhPPA. Working with a reagent concentration of 7.5 mM it can be assumed that the PhPPA/DPPA ratio is the same in the reaction mixture and on the surface. Additional ^{1}H NMR experiments in which the nanoparticles were dissolved in HF and the resulting mixture was extracted with deuterated chloroform support this assumption. Integration of the NMR-signals revealed that at a concentration of 7.5 mM the found ratio after surface degrafting represented in all cases (<25% deviation) the mixing ratio of the capping agents in the solution before the reaction.

TGA analyses revealed that a total grafting density of 2.8 ± 0.6 molecules/nm^2 with increasing PhPPA percentage could be reached for the prepared mixed modified samples. The grafting density is higher than for the solely DPPA-grafted particles. A possible explanation for this behavior is that the smaller more reactive PhPPA molecules bind to sites where DPPA cannot bind, e.g. defect sites.

FT-IR-spectroscopy was again used for the determination of the degree of ordering of the C12-alkyl chains in dependence of the mixture of molecules on the surface. Fig. 6 shows the overlayed spectra for the C—H-stretching region. It reveals that with increasing PhPPA-concentration on the particle surface the methylene C—H-vibration (ν_{as} as example) shifts significantly to higher wavenumbers. Thus the ordering of the C12-chains decreases (Fig. 7). To verify the effectiveness of our approach also for crystalline SAM-systems, C18-chain-mixed-systems have been investigated in the same way.

Fig. 7 shows an increase of alky-chain ordering by increasing the percentage of long alkyl chain capping agent in the mixed surface layer. This effect has qualitatively the same trend for C12 and C18. Only the absolute values differ, which means that the C12 groups are generally more disordered compared to the C18 system, which is crystalline at room temperature [17]. Therefore this mixed monolayer alkyl chain disordering approach is applicable for crystalline ordered and medium ordered SAMs. Scheme 1 visualizes the mixed SAM formation on the zirconia surface.

The DPPA and ODPPA curves in Fig. 7 show two different regions, a flat slope at higher long alkyl chain capping agent concentrations and a linear steep slope in SAM ordering for high PhPPA concentrations. These two regions are most likely due to the competition of different SAM growth mechanisms. In a first step the attachment of the molecules occurs randomly all over the particle surface. In the second step an island type growth of ordered

regions can be expected [41]. But there is no information on the growth mechanism of this mixed coupling agent monolayer and as the IR peaks represent a statistical average over all attached species it is likely to be a combination of effects that leads to the shifts, which makes the system rather complex and does not allow to distinguish between the mechanisms.

However, it is clear that the PhPPA attachment to the surface can disturb the DPPA monolayer formation. This can be explained by adsorpion of molecule by molecule which leads to a mixed surface layer where the PhPPA/DPPA molecules are randomly mixed, as observed for mixed alkyl thiols on gold with different chain lengths [42,43]. The second extremum, intense macroscopic island formation as discussed by Bain et al. [44,45] and investigated by Vercelli et al. [46] for strongly interacting co-capping agents is not very likely because there would be no effect on the disordering of the (amorphous) ordered C12 chains. A mechanism in between these extrema is likely to be existent, e.g. such as the formation of islands in the nanometer range in the case of octadecylphosphonic acid on mica [47]. Also a pre-formation of coupling agent assemblies in solution by weak interactions before adsorption to the surface is possible in analogy to the covalently crosslinked structures of trialkoxysilanes. Driving forces for such a mechanism are the chain-crystallization energy of long alkyl chains or the π–π-interaction [3,4] for PhPPA. This is only possible if the compounds have a natural tendency to form preordered structures in solution before surface-attachment as it is observed in literature for functional long alkyl chain phosphonic acids [48].

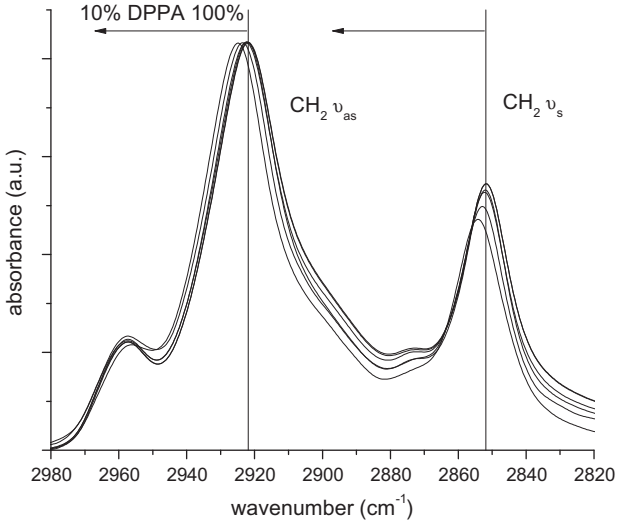

Fig. 6. Infrared spectra of DPPA/PhPPA@ZrO_2: methylene C—H shifts to higher wavenumber at increasing PhPPA surface concentration.

3.5. Zirconia: dispersibility of mixed modified nanoparticles

As discussed above, the mixed monolayer formation at the nanoparticle surface should enhance the dispersibility in organic solvents. We investigated this effect by dispersing the nanoparticles in an organic solvent (*n*-hexane) using the same procedure which is applied when nanoparticles are dispersed in monomers for nanocomposite syntheses via *in situ*-polymerization [2,49,50]. A simple ultrasonic bath (treatment for 30 min) was used for dispersing the dry nanoparticle powder in the solvent to obtain 0.5 g/L dispersions. The dispersions were allowed to equilibrate for 1 h and afterwards the quality of the dispersions was evaluated by DLS-measurements. Fig. 8 shows the size distribution of mixed modified nanoparticles containing 90% and 70% DPPA as well as 100% DPPA. The surface weighted distribution function is shown because the interface region is crucial in inorganic–organic nanocomposites.

Each measured distribution is bimodal with the peak at lower radii representing the single nanoparticles (see also Fig. 3) and most likely the peak at larger radii is resulting from agglomerates. The 100% DPPA-system shows the largest size distribution in case of small radii and larger agglomerates (around 0.5 μm), which is a strong indication for agglomeration in suspension. The peak at lower radii sharpens for the particles with 90% DPPA and 70% DPPA. In addition the peak for the larger agglomerates shifts to lower radii and narrows, which can be due to a decrease of agglomerate sizes and also a change of the hydrodynamic behaviour of the different modified particles. In the case of 70% DPPA concentration again a slight broadening of this second peak is observed and for the 50% system (not shown), the dispersion quality again decreases dramatically showing huge agglomerate peaks. This is considered to be due to the fact that DPPA is the major molecule that hydrophobizes the surface and thus enhances the interaction with the non-polar solvent. If the surface is only partially covered with

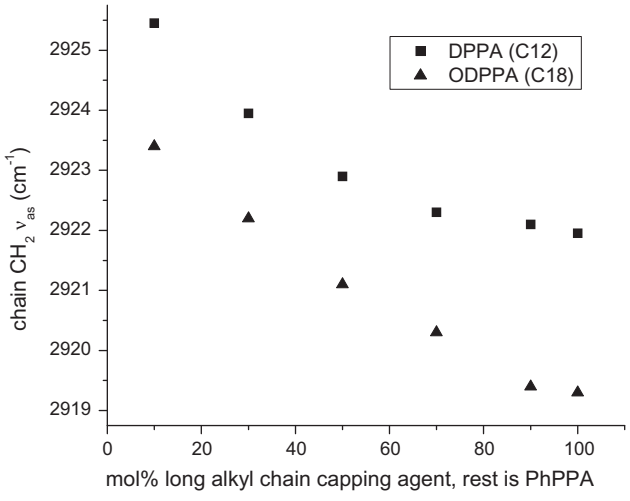

Fig. 7. Methylene C—H-vibration ν_{as} of long alkyl chain-PPA@ZrO_2 representing the alkyl-chain ordering degree at different percentages of DPPA or ODPPA (rest PhPPA).

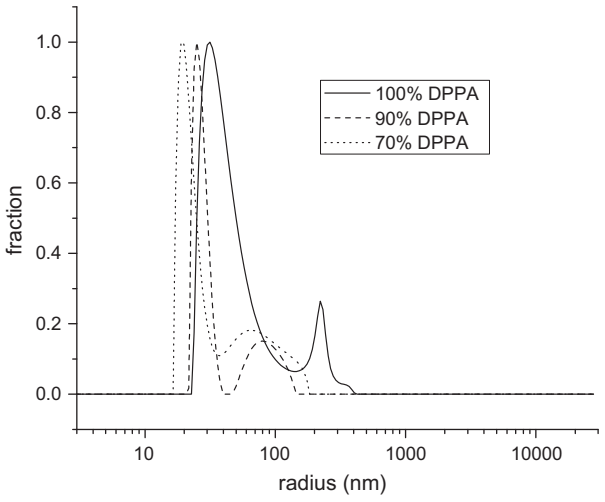

Fig. 8. Surface weighted size distribution of mixed modified ZrO_2 nanoparticles (from DLS-measurements), dispersed in *n*-hexane via ultrasonic treatment.

DPPA, the dispersion quality is as poor as for the analogous system with 100% PhPPA in *n*-hexane.

Thus, there is an optimum in dispersibility for a PhPPA-content of 10–30%. This fact is likely to originate from the described agglomeration effect by interparticle alkyl bilayer formation. The alkyl-chain ordering (see C—H-shifts in Fig. 7), is already affected at PhPPA contents of 10–30% which may result in better deagglomeration properties, because agglomerates from more oriented alkyl chain systems are more stable [12,51] and therefore more difficult to break. This effect of chain ordering on dispersion behavior is plausible as Sahoo et al. described that disordered monolayers like that of oleic acid on nanoparticles compared to monolayers of hexadecane phosphonic acid show better dispersibility because the latter form bilayer structures [52].

The hypothesis that the surface alkyl ordering affects the dispersibility is also justifiable because one would expect in an alkane medium like *n*-hexane that the particles are better dispersible if the DPPA content increases since the alkyl chains of the solvent better interact with the dodecyl chains than with phenyl-residues. This incompatibility may be the reason for a decrease of dispersibility at higher PhPPA contents (50%). However, the liquid *n*-hexane molecules can better interact with more disordered surface alkyl chains than with strongly ordered systems [52], which would explain the observed dispersibility optimum.

In literature, gold nanoparticles have been modified with binary mixtures of alkylthiols to tune interparticle spacing of particle deposits [18] and Kubowicz et al. [7] used a mixed monolayer approach by Glogowski et al. [53] via ligand exchange to fine-tune the wettability properties of these particles. We expect that similar mechanisms which we describe here are responsible for their results, however no alkyl-chain ordering has been studied in their work. Usually there is a strong correlation of wettability and alkyl chain packing [54].

Applying this mixed monolayer approach, an improvement of the dispersion quality of the C12 modified ZrO_2 nanoparticles in hexane by disturbing the C12 chain ordering while maintaining full nanoparticle surface coverage could be reported. The C18 (ODPPA) modified nanoparticles did not give stable dispersions applying the same approach.

3.6. Silica: particle size and alkyl-chain ordering

Contrary to nanocrystalline zirconia the silica particles have a spherical nature and thus the nanoscopic curvature has an influence on the SAM-formation. Jones et al. have shown by modifying 7 nm, 12 nm, and 40 nm diameter spherical silica particles using different alkyl chain-length silane coupling agents ($n = 8$, 10, 12, 18) that the chain packing decreases for lower diameter particles due to the increased curvature which prevents a continuous parallel packing of the alkyl chains as it would be possible for flat surfaces [9]. As described above crystalline 22 nm zirconia particles of similar size ranges show quite strong ordering phenomena in long-alkyl chain phosphonate interaction, based on the defined flat crystal facets of the nanocrystals.

SAM formation and disordering was proven applying SiO_2 samples with different sizes and thus variations in surface curvature. The surface functionalization was carried out using a two step process. First a *Stöber*-process was used to synthesize well-defined particles followed by a surface-modification step with the silane coupling agent DTMS. Organophosphorous coupling agents could not be used in this case because they do not interact with silica surfaces by strong covalent bonds. Trialkoxysilane based coupling agents and not mono alkoxysilanes were used in surface-modifications, because the application of trifunctional silanes results in SAMs with grafting densities and chain ordering more comparable to the phosphonate systems [21]. Other reaction parameters, such as temperature and coupling agent concentration, were also chosen to be comparable with the phosphonate surface-modifications. The resulting grafting densities (~2 molecules/nm^2) were similar to those of the zirconia particles. But they could not be exactly determined by the method used for the zirconia nanoparticles because of the possible ultrastructure of *Stöber*-particles and potential residual surface-ethoxy groups from the preparation (see solid state NMR spectra in Supplementary data). These conditions are in contrast to common methods, used in chlorosilane- or alkoxysilane-treatment of metal oxide surfaces in nonpolar aprotic media, which occur mostly at elevated temperatures [55–58]. SiO_2-particles with four different diameters have been prepared and surface-modified with DTMS. Table 3 lists the particle diameters and the corresponding methylene-C—H-vibration from IR-investigations. Compared to the value for C—H ν_{as} for C12@hydroxylated Si(1 0 0) of 2920.9 cm^{-1} [9] which should represent the maximum ordered C12 chain-packing of silica surfaces, the alkyl chains at the nanoparticle surfaces are much less ordered showing a liquid like behavior. Also the C12 monolayer on the hydroxylated Si-wafer from our experiment shows less ordered structure compared to literature [9]. The reason for this is considered to be that the solvent mixtures used, namely water/ethanol or water/methanol, leads to more disordered monolayers as nonpolar media. However these conditions were necessary to yield a sample, comparable to the functionalized zirconia nanoparticle powders. Fig. 9 shows the alkyl-chain ordering at the nanoparticle surface in dependence of the particle size revealing the influence of the curvature on the SAM-formation.

The ordering of C12 chains at the surface increases for higher particle diameters and thus for lower curvatures which was also shown by Jones et al. We extended their study from nanoparticles to micron-sized particles and flat substrates. The 680 nm particles should already mimic the SAM formation on flat surfaces which can be concluded from a comparison of the C—H-stretching vibrations. The nanoparticles at 9 and 46 nm diameter follow the trend, observed by Jones et al. The data points for the 390 and 680 nm diameter do not represent the same trend. A possible explanation for this trend is that *Stöber* particles have a fractal particle structure by nature due to the preparation process [59] (e.g. 3 nm close packed nanoparticles [60]). For this reason, the outer surface is never totally flat, as Szekeres et al. showed by comparison of SAXS and BET data. For the trend in the diagram in Fig. 9 this would mean that for higher nanoparticle diameters the "surface roughness" is lower (in the TEM-image in Fig. 2) than for the smaller nanoparticles which results in a better ordered monolayer. These differences in surface roughness are the result of the different synthetic conditions, which were necessary to be varied to produce particles with different diameters. The variation of the synthetic parameters (primarily ratios of the educts) influences the nucleation rate and thus the primary particle size during the Stöber process [61]. For example, it can be observed that for a higher water-content at the same ammonia concentration, the Stöber-particle surface appears more rough in electron micrographs [62]. However, this surface structure does not seem to play a role

Table 3
Dodecyl chain methylene C—H-vibration ν_{as} of DTMS@silica particles with different diameter and on a flat substrate.

d(DLS), m.w. (nm)	C—H ν_{as} (cm^{-1})
9	2929
46	2928
390	2927
680	2925
∞	2925

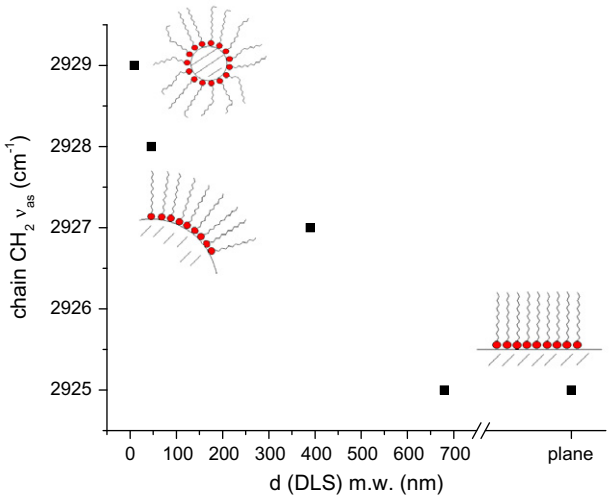

Fig. 9. Methylene C—H-vibration ν_{as} of DTMS@SiO_2 representing alkyl-chain ordering degree at different particle curvatures.

for the 680 nm particle as the same C12 methylene vibrational shifts are observed as for the atomar flat wafer substrate, which means that the surface of the 680 nm particles can be considered flat for the capping agent molecules.

It is concluded that the curvature has a stronger influence on the ordering as expected however it is not easy to determine a real curvature effect which is responsible for an alkyl chain disordering effect, a possible ultrastructure (surface roughness or smaller local radius) of the nanoparticles has to be taken into account. But it can be concluded that the smaller the overall surface curvature the higher is the degree of ordering. Therefore our study shows an extension of the results previously reported in literature for small SiO_2 nanoparticles [9]. The values for the methylene C—H for DTMS@silica nanoparticles of 2929–2928 cm^{-1} indicate a nearly liquid like unordered surface alkyl-chain system [30] in contrast to 2925 cm^{-1} for DTMS@silica micron-sized particles which point towards a far more ordered, but not as densely packed as e.g. for C18 on planar and slightly curved silica [63], SAM structure. It can be considered that by using DTMS@silica nanoparticles in nanocomposites no zipper-effect will occur which results in bilayer formation at the interface between two particles.

The grafting densities have been investigated by thermal analysis and showed values of ~1.1 molecules/nm^2 for the 46 nm particles and ~1.7 molecules/nm^2 for the largest 680 nm diameter particles. TGA studies in this case provide only a limited precision due to the mass loss of remaining silane alkoxide groups. However, there is a qualitative agreement with the observed ordering of the C12-chains: high chain ordering allows higher grafting densities.

3.7. Silica: alkyl chain disordering by co-modification

The generality of our approach in breaking the order of SAM formation on particle surfaces by applying different surface coupling agents was tested by using the DTMS-modified submicron-sized silica particles (680 nm diameter). Mixing of PhTMS with DTMS in surface modification of the particles should lead to a decrease of ordering in the chain packing. The surface-functionalization method was similar as described for zirconia. The overall molar coupling agent concentration was kept constant while the ratio of DTMS/PhTMS was varied. The degree of alkyl-chain ordering was analyzed via FT-IR-spectroscopy and the methylene C—H shift for each percentage of C12-chain@SiO_2 is visualized in the diagram in Fig. 10.

The alkyl-chain ordering of DTMS@silica decreases with increasing percentages of PhTMS showing a similar trend as observed for the DPPA/PhPPA@ZrO_2 system. Comparison of the two systems (Figs. 7 and 10) reveals that in both cases a more or less linear trend for the decrease of ordering from 100%C12 to 10%C12 is observable with a total shift of ~5 cm^{-1}. The wavenumber of the most disordered state for silica particles is ~2930 cm^{-1} and for zirconia ~2925 cm^{-1}, which means that the chain-ordering in absolute is higher for the zirconia system. The entire ordering curve (Fig. 10) is shifted to lower wavenumbers as compared to the zirconia system (Fig. 7). A possible ultrastructure of the *Stöber*-particle-surface yielding in higher disordering may also be responsible for this fact. Also these two systems, phosphonates@ZrO_2 and trialkoxysilanes@SiO_2 are not comparable one-to-one for phosphonates the modification reaction is represented by an adsorption of molecule by molecule whereas trialkoxysilanes pre-form aggregates via self condensation in solution which then adsorb to the nanoparticle surface. The later effect can also be responsible for the quantitative differences in chain-ordering of these two systems.

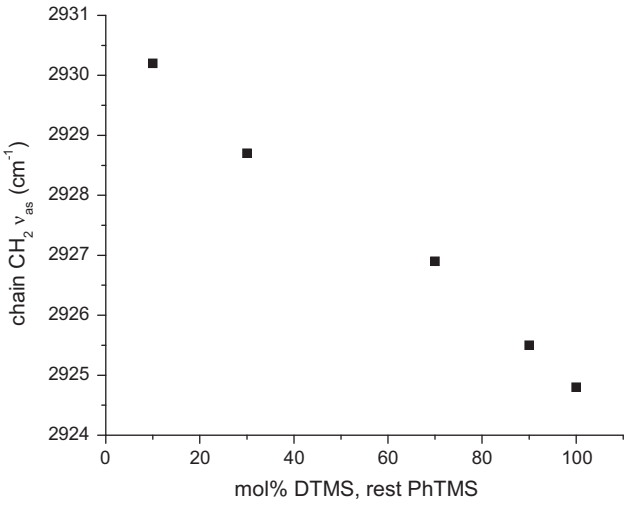

Fig. 10. Methylene C—H-vibration of DTMS@SiO_2 680 nm diameter representing alkyl-chain ordering degree at different percentages of DTMS (rest PhTMS).

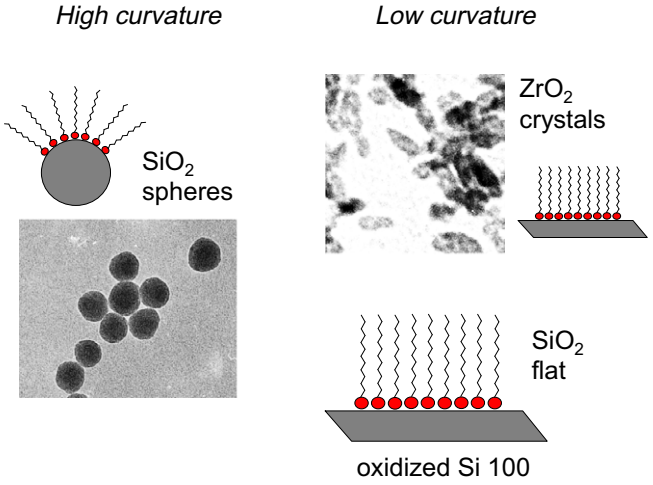

Fig. 11. Schematic representation of dodecyl-chains adsorbed on zirconia/silica showing different nanoscopic curvature: comparison of C12@zirconia nanocrystals with C12@spherical silica nanoparticles in the same size range (10–40 nm): zirconia nanoparticles reveal highly ordered SAM due to plane crystal facets whereas spherical silica nanoparticles show no strong ordering of alkyl chains.

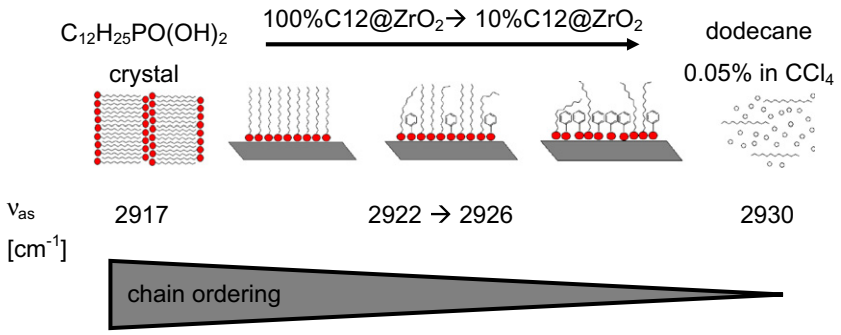

Scheme 1. Schematic representation of different C_{12}-alkyl chain-ordering-degrees at the zirconia nanoparticle surface and comparison with totally crystalline C_{12}-chains and high diluted unordered liquid C_{12}-chains.

Nevertheless the effect of binding of a co-coupling agent shows qualitatively and quantitatively a similar effect regardless of the different curvatures and chemical surface properties of the particle systems and the chemical behavior of the different capping agents.

4. Conclusions

We have investigated the ordering behavior of dodecyl chains on plane-crystal-shaped zirconia nanoparticles and on spherical silica particles with phosphonate or alkoxysilane anchor groups. The CH-vibrations of the alkyl chain methylene-units in FT-IR-studies were used to detect the degree of alkyl chain packing in the self-assembled-monolayer (SAM) of the surface bonded long-alkyl-chain molecule. The highly ordered SAM can be responsible for significant changes in physical particle surface properties and influence the tendency of the particles to agglomerate via interparticle alkyl-chain-bilayer formation, and thus destabilization of nanoparticle dispersions, which is undesirable for many applications, such as nanocomposite preparation. This can be a problem for facets of larger size (upper nm range to macroscopic scale) as it is the case for zirconiumalkylphosphonate-films [23], because the stability of the alkyl bilayer is given by the number of *Van der Waals* – interacting alkyl chains. However this occurs also for very small nanoparticles, as described in literature, a strong intercalation of chains can occur to compensate the high surface curvature, e.g. long-alkyl-chains on 2 nm gold nanoparticles/clusters [51] are highly ordered and hydrocarbon- as well as fluorocarbon-chains on 4 nm zirconia nanoparticles are stronger ordered than on 20 nm zirconia particles [8].

It was shown that for SiO_2-particles in the lower nanometer length scale the SAM-effect does not play a role, because of the particles' high curvature, which seems to be still high enough that chain intercalation does not increase because of surface energy compensation. Zirconia nanocrystals in the same size range displaying plane surfaces form ordered SAMs of dodecylchains because the surface in these samples mimic flat ideal crystal surfaces which enhances a dense chain packing.

Thus the nanoscopic curvature of the particles is crucial for the occurrence of alkyl-chain ordering occurs or not (Fig. 11). But it was also shown for both systems, silica and zirconia, that mixed monolayer formation of long alkyl-chains (dodecyl-moiety) with a small, disturbing coupling agent (phenyl-moiety) at a certain total grafting density gives less ordered alkyl-chains at the nanoparticle surface. This is important in terms of nanoparticle surface engineering where highly ordered surface-SAMs have to be avoided because of possible interparticle bilayer formation and thus the formation of thermodynamically very stable agglomerates of the nanoparticles.

Nanoparticle-SAM effects stick to the rules of well investigated SAM-effects on macroscopic flat surfaces such as SiO_2 on Si wafers, except for the presence of an ultrastructure with high curvature, e.g. *Stöber*-particles. Although the systems of SiO_2 and ZrO_2 should not be compared directly because different surface modifying anchor groups are used with different adsorption behavior it is obvious that for both different systems the nanoscopic curvature is important for the formed alkyl-surface-layer structure (Fig. 11) and co-adsorbtion of other capping agents with different organic moieties yields in disorientation of long alkyl chains in both cases.

This study shows on the basis of the investigated compounds that the nanoscopic curvature has an impact on the surface-properties itself. Furthermore, by variation of the grafting density or by mixed SAM-formation at full surface coverage, the surface properties of metal oxide nanoparticles can be controlled on a molecular level.

Acknowledgments

The Austrian Science Fund (FWF, Project Nr. P20693) is gratefully acknowledged for the financial support of this work. The authors thank Dr. Berthold Stöger and Dr. Robert Haberkorn for XRD measurements and the University Service Center for Transmission Electron Microscopy, Vienna University of Technology, for help with recording TEM-images. Additional thanks goes to Dr. Michael Puchberger for solid state NMR-measurements and to Anders Hendriksson for his help with silicon wafer preparation and monolayer characterization.

Appendix A. Supplementary material

Supplementary data, including information from nitrogen sorption-, powder-XRD-, solid state NMR- experiments as well as the corresponding data tables to the depicted figures, associated with this article can be found, in the online version, at doi:10.1016/j.jcis.2011.03.035.

References

[1] M.-A. Neouze, U. Schubert, Monatsh. Chem. 139 (2008) 183.
[2] G. Kickelbick, Prog. Polym. Sci. 28 (2003) 83.
[3] S. Onclin, B.J. Ravoo, D.N. Reinhoudt, Angew. Chem., Int. Ed. 44 (2005) 6282.
[4] A. Ulman, Chem. Rev. 96 (1996) 1533.
[5] M.K. Corbierre, N.S. Cameron, R.B. Lennox, Langmuir 20 (2004) 2867.
[6] P. Fiurasek, L. Reven, Langmuir 23 (2007) 2857.
[7] S. Kubowicz, J. Daillant, M. Dubois, M. Delsanti, J.-M. Verbavatz, H. Mohwald, Langmuir 26 (2010) 1642.
[8] A. O'Donnell, K. Yach, L. Reven, Langmuir 24 (2008) 2465.
[9] R.L. Jones, N.C. Pearsall, J.D. Batteas, J. Phys. Chem. C 113 (2009) 4507.
[10] A. Badia, L. Demers, L. Dickinson, F.G. Morin, R.B. Lennox, L. Reven, J. Am. Chem. Soc. 119 (1997) 11104.
[11] M. Fukuto, R.K. Heilmann, P.S. Pershan, A. Badia, R.B. Lennox, J. Chem. Phys. 120 (2004) 3446.

[12] R.H. Terrill, T.A. Postlethwaite, C.-h. Chen, C.-D. Poon, A. Terzis, A. Chen, J.E. Hutchison, M.R. Clark, G. Wignall, et al., J. Am. Chem. Soc. 117 (1995) 12537.
[13] L. Chen, J. Xu, J.D. Holmes, M.A. Morris, J. Phys. Chem. C 114 (2010) 2003.
[14] Y. Min, M. Akbulut, K. Kristiansen, Y. Golan, J. Israelachvili, Nat. Mater. 7 (2008) 527.
[15] P.H. Mutin, V. Lafond, A.F. Popa, M. Granier, L. Markey, A. Dereux, Chem. Mater. 16 (2004) 5670.
[16] W. Gao, L. Dickinson, C. Grozinger, F.G. Morin, L. Reven, Langmuir 12 (1996) 6429.
[17] W. Gao, L. Dickinson, C. Grozinger, F.G. Morin, L. Reven, Langmuir 13 (1997) 115.
[18] A. Rezaee, L.C. Pavelka, S. Mittler, Nanoscale Res. Lett. 4 (2009) 1319.
[19] M.C. Prado, B.R.A. Neves, Langmuir 26 (2010) 648.
[20] S. Brunauer, P.H. Emmett, E. Teller, J. Am. Chem. Soc. 60 (1938) 309.
[21] A.Y. Fadeev, R. Helmy, S. Marcinko, Langmuir 18 (2002) 7521.
[22] G.M. Kosolapoff, J. Am. Chem. Soc. 66 (1944) 109.
[23] T. Vallant, H. Brunner, U. Mayer, H. Hoffmann, Langmuir 14 (1998) 5826.
[24] W. Stoeber, A. Fink, E. Bohn, J. Colloid Interface Sci. 26 (1968) 62.
[25] Y. Murase, E. Kato, J. Am. Ceram. Soc. 84 (2001) 2705.
[26] G. Guerrero, P.H. Mutin, A. Vioux, Chem. Mater. 13 (2001) 4367.
[27] S. Marcinko, A.Y. Fadeev, Langmuir 20 (2004) 2270.
[28] M.L. Hair, C.P. Tripp, Colloids Surf., A 105 (1995) 95.
[29] F. Brodard-Severac, G. Guerrero, J. Maquet, P. Florian, C. Gervais, P.H. Mutin, Chem. Mater. 20 (2008) 5191.
[30] R. Helmy, A.Y. Fadeev, Langmuir 18 (2002) 8924.
[31] R. Bautista, N. Hartmann, E. Hasselbrink, Langmuir 19 (2003) 6590.
[32] W.G. Golden, C.D. Snyder, B. Smith, J. Phys. Chem. 86 (1982) 4675.
[33] R.G. Snyder, H.L. Strauss, C.A. Elliger, J. Phys. Chem. 86 (1982) 5145.
[34] J. Randon, P. Blanc, R. Paterson, J. Membr. Sci. 98 (1995) 119.
[35] P.S. Haddad, T.R. Rocha, E.A. Souza, T.M. Martins, M. Knobel, D. Zanchet, J. Colloid Interface Sci. 339 (2009) 344.
[36] R. Mueller, H.K. Kammler, K. Wegner, S.E. Pratsinis, Langmuir 19 (2003) 160.
[37] D.M. Spori, N.V. Venkataraman, S.G.P. Tosatti, F. Durmaz, N.D. Spencer, S. Zuercher, Langmuir 23 (2007) 8053.
[38] F. Bellezza, A. Cipiciani, M.A. Quotadamo, Langmuir 21 (2005) 11099.
[39] M.D. Porter, T.B. Bright, D.L. Allara, C.E.D. Chidsey, J. Am. Chem. Soc. 109 (1987) 3559.
[40] D.A. Offord, J.H. Griffin, Langmuir 9 (1993) 3015.
[41] M.L. Schilling, H.E. Katz, S.M. Stein, S.F. Shane, W.L. Wilson, S.B. Ungashe, G.N. Taylor, T.M. Putvinski, C.E.D. Chidsey, S. Buratto, Langmuir 9 (1993) 2156.
[42] J.P. Folkers, P.E. Laibinis, G.M. Whitesides, Langmuir 8 (1992) 1330.
[43] P.E. Laibinis, R.G. Nuzzo, G.M. Whitesides, J. Phys. Chem. 96 (1992) 5097.
[44] C.D. Bain, J. Evall, G.M. Whitesides, J. Am. Chem. Soc. 111 (1989) 7155.
[45] C.D. Bain, G.M. Whitesides, Science 240 (1988) 62.
[46] B. Vercelli, G. Zotti, G. Schiavon, S. Zecchin, A. Berlin, Langmuir 19 (2003) 9351.
[47] J.T. Woodward, A. Ulman, D.K. Schwartz, Langmuir 12 (1996) 3626.
[48] D. Francova, G. Kickelbick, Monatsh. Chem. 14 (2009) 413.
[49] W.R. Caseri, Mater. Sci. Technol. 22 (2006) 807.
[50] M.M. Demir, P. Castignolles, U. Akbey, G. Wegner, Macromolecules 40 (2007) 4190.
[51] A. Badia, L. Cuccia, L. Demers, F. Morin, R.B. Lennox, J. Am. Chem. Soc. 119 (1997) 2682.
[52] Y. Sahoo, H. Pizem, T. Fried, D. Golodnitsky, L. Burstein, C.N. Sukenik, G. Markovich, Langmuir 17 (2001) 7907.
[53] E. Glogowski, J. He, T.P. Russell, T. Emrick, Chem. Commun. (2005) 4050.
[54] S.A. Kulinich, M. Farzaneh, Appl. Surf. Sci. 230 (2004) 232.
[55] M. Khayet, J.P.G. Villaluenga, J.L. Valentin, M.A. Lopez-Manchado, J.I. Mengual, B. Seoane, Polymer 46 (2005) 9881.
[56] J.D. Le Grange, J.L. Markham, C.R. Kurkjian, Langmuir 9 (1993) 1749.
[57] P. Silberzan, L. Leger, D. Ausserre, J.J. Benattar, Langmuir 7 (1991) 1647.
[58] P.M. St. John, H.G. Craighead, Appl. Phys. Lett. 68 (1996) 1022.
[59] D.L. Green, J.S. Lin, Y.-F. Lam, M.Z.C. Hu, D.W. Schaefer, M.T. Harris, J. Colloid Interface Sci. 266 (2003) 346.
[60] P.J. Davis, R. Deshpande, D.M. Smith, C.J. Brinker, R.A. Assink, J. Non-Cryst. Solids 167 (1994) 295.
[61] K. Lee, A.N. Sathyagal, A.V. McCormick, Colloids Surf., A 144 (1998) 115.
[62] S.K. Park, K.D. Kim, H.T. Kim, Colloids Surf., A 197 (2002) 7.
[63] S.A. Kulkarni, S.A. Mirji, A.B. Mandale, K.P. Vijayamohanan, Thin Solid Films 496 (2006) 420.